Available online at www.sciencedirect.com
SCIENCE DIRECT®
Journal of Solid State Chemistry 177 (2004) 2575–2583
JOURNAL OF SOLID STATE CHEMISTRY
http://elsevier.com/locate/jssc

New binuclear vanadium(III) and (IV) squarate species: synthesis, structure and characterization of $[V(OH)(H_2O)_2(C_4O_4)]_2 \cdot 2H_2O$ and $(NH_4)[(VO)_2(OH)(C_4O_4)_2(H_2O)_3] \cdot 3H_2O$

C. Brouca-Cabarrecq,* A. Mohanu, P. Millet, and J.C. Trombe

Centre d'Elaboration de Materiaux (CEMES/CNRS) et d'Etudes Structurales du CNRS, 29 rue Jeanne Marvig, B.P. 4347, 31055 Toulouse Cedex 4, France

Received 19 May 2003; received in revised form 8 July 2003; accepted 12 July 2003

Abstract

Two new vanadium squarates have been synthesized, characterized by infrared and thermal behavior and their structures determined by single crystal X-ray diffraction. Both structures are made of discrete, binuclear vanadium entity but in **1**, $[V(OH)(H_2O)_2(C_4O_4)]_2 \cdot 2H_2O$ the vanadium atom is trivalent and the entity is neutral while in **2**, $(NH_4)[(VO)_2(OH)(C_4O_4)_2(H_2O)_3] \cdot 3H_2O$, the vanadium atom is tetravalent and the entity is negatively charged, balanced by the presence of one ammonium ion. Both molecular anions are bridged by two terminal μ_2 squarate ligands. **1** crystallizes in the triclinic system, space group P-1, with lattice constants $a = 7.5112(10)$ Å, $b = 7.5603(8)$ Å, $c = 8.2185(8)$ Å, $\alpha = 106.904(8)^\circ$, $\beta = 94.510(10)^\circ$, $\gamma = 113.984(9)^\circ$ while **2** crystallizes in the monoclinic system, space group $C2/c$, with $a = 14.9340(15)$ Å, $b = 6.4900(9)$ Å, $c = 17.9590(19)$ Å and $\beta = 97.927(12)^\circ$. From the magnetic point of view, V(III) binuclear species show ferromagnetic interactions at low temperatures. However, no anomalies pointing to magnetic ordering are observed down to 2 K.

Keywords: Vanadium; Squarate; Synthesis; Structure; Characterization

1. Introduction

There has been an extensive interest in vanadium compounds due to their numerous applications and properties. For example, such compounds and particularly oxides are interesting as active cathode materials in reversible lithium ion batteries. This fact results from their good electrochemical characteristics, including mixed ionic and electronic conduction properties [1]. Most of the syntheses were realized by traditional high temperature solid-state chemistry [2] and consequently the lithium diffusion was somehow hindered due to the compactness of these phases. It would be then interesting to use new synthetic approaches that would lead to "open-framework" structure in order to increase lithium mobility. Hydrothermal syntheses, using an organic ligand as templating agent, have proved to be a successful method to achieve this goal. The better known open-framework structures, namely aluminosilicates and phosphates (zeolites, aluminophosphates, gallophosphates, …), have been generally based on tetrahedral connectivity. For the past 10 years, various attempts have been made to replace these species by an organic ligand, for example a dicarboxylic acid that would act as a building unit to form a porous structure [3].

It is worth to mention that open-framework networks have been obtained in the case of the cobalt-squarate [4] and that Cheetham and co-workers have recently analyzed a structure based on metal squarates which, from the structural point of view, was compared to sodalite [5]; this structure was previously determined by Weiss [6]. The system vanadium/squarate has been chosen, anticipating that new topologies could be obtained, in which porosity, electrical or magnetic properties will be enhanced. Squaric acid has been selected because it contains delocalized π electrons and consequently it could favor long range super exchange coupling [7].

*Corresponding author. Fax: +05-62-25-7999.
E-mail address: brouca@cernes.fr (C. Brouca-Cabarrecq).

0022-4596/$ - see front matter © 2003 Elsevier Inc. All rights reserved.
doi:10.1016/S0022-4596(03)00396-7

Some compounds have already been obtained in the system vanadium/squarate [8–11] but it appears that new possibilities can be explored. Here, we report the synthesis and characterization of two new compounds $[V(OH)(H_2O)_2(C_4O_4)]_2 \cdot 2H_2O$ **1**, $(NH_4)[(VO)_2(OH)(C_4O_4)_2(H_2O)_3] \cdot 3H_2O$ **2**. Similarities and differences between the two structures will be emphasized and then a comparison with some similar structures, reported in the literature, will be made [8,9,11].

2. Experimental section

2.1. General information

X-ray powder diffraction measurements were recorded on a Seifert diffractometer using Cu$K\alpha$ radiation. The theoretical X-ray diffraction patterns were calculated using the Lazy Pulverix program [12]. Thermogravimetric analyses were performed in the temperature range 20–500°C at a heating rate of 5°C min^{-1} under O_2 atmosphere, using a Setaram apparatus. IR spectra were recorded between 4000 and 400 cm^{-1} on a Perkin-Elmer 1725X FT-IR spectrometer. Samples were run as KBr pellets.

2.2. Synthesis

The syntheses were performed under hydrothermal conditions, under autogenous pressure. Compound **1**: an aqueous suspension (10 mL) of V_2O_5 (1 mmol) and $H_2(C_4O_4)$ (4 mmol) was heated in a Teflon-lined steel bomb. After 3 days at 150°C, the mixture was filtered off, washed with water and air-dried. Brown crystals were isolated. The pH of the solution after heating was equal to 2. Monophasic crystalline material was confirmed by X-ray powder diffraction. Elemental analysis leaded to the following values %: calcd. C 20.5, H 2.99, % found C 20.7, H 2.54. Willing to obtain some organic–inorganic hybrid materials, in which the ethylenediamine would act as a template, the last reactant was added in the starting solution. Nonetheless, the same pure phase was observed whether ethylenediamine was present or not.

Compound **2**: as for compound **1**, the first two reactants were the same V_2O_5 (1 mmol.) and $H_2C_4O_4$ (4 mmol.), but some ammonium fluoride was added in the aqueous suspension, in different molar ratios, $F/V = 1.5$ and 3. After a thermal treatment as for compound **1** and whatever the F/V ratio, only a limpid green–blue solution, whose pH ranged from 3.3 to 4.5, was obtained with no evident traces of powder or crystallites. This solution was evaporated for a few days, at room temperature. It is worthwhile to notice a color change of this solution during the evaporation: starting from green–blue it became blue and then brown. At nearly the end of evaporation, some crystals were observed. They were washed with a limited amount of distilled water, since they are soluble in an excess of water, and air-dried. Optical microscopic examination indicated that three types of crystals or powder were present: numerous green–black crystals (compound **2**) which were intermixed with white powder or crystallites and a few tiny blue crystallites (see Section 3 below). The X-ray powder diffraction pattern showed the presence of two phases: the first one is representative of the theoretical diagram for **2** and the second corresponding to ammonium fluoride. The chemical analysis of selected green–black crystals led to the following values: C 19.4%; N 3.0%, H 3.3%. Calculated values for the compound **2** are: C 19.17%; N 2.80%, H 3.42%. Electron energy loss spectroscopy (EELS) of carefully selected green–black crystals (compound **2**) confirmed firstly the absence of the fluoride ion and secondly that the atomic ratio of N/V was around 1/2. These results were coherent with the weight loss of selected green–black crystals (see Section 3.3).

2.3. Magnetic measurement

Only the results concerning form **1** will be presented, owing to the difficulty to isolate suitable amount of clean single crystals of form **2**. Susceptibility (sweep two temperature mode, field intensity 5 kG) was performed in the temperature range 2–300 K on selected single crystals using a SQUID magnetometer MPM5-5 quantum design.

2.4. X-ray structure determination

The diffraction data were collected using an Enraf Kappa-CCD automatic X-ray single crystal diffractometer. This goniometer is equipped with a planar area detector allowing a quick measurement of the whole diffraction sphere. The refined cell constants and additional relevant crystal data are given in Table 1.

For both compounds, the structure solution was found using SIR 92 [13]. The intensity data were corrected for absorption using a "multi-scan" technique [14]. Hydrogen atoms were located from successive difference Fourier maps and were riding at their relevant parent atoms. The refinements were carried out using anisotropic thermal displacements for all the non-hydrogen atoms. For compound **1**, the refinements were performed using the least-squares methods included in MAXUS [15] while for **2**, the program SHELXL-97 was used [16].

For compound **2**, the bimetallic vanadium entity is one time negatively charged, due to the presence of both oxo-vanadium(IV) atoms and one hydroxyl ion which was localized on the binary axis. Consequently, one of the two sites, not pertaining to

Table 1
Crystallographic data and structure refinement for $[V(OH)(H_2O)_2(C_4O_4)]_2 \cdot 2H_2O$ **1**, and for $(NH_4)[(VO)_2(OH)(C_4O_4)_2(H_2O)_3] \cdot 3H_2O$ **2**

Compound	**1**	**2**
Crystal system	Triclinic	Monoclinic
Space group	*P*-1	*C*2/*c*
Temperature (*K*)	298	298
Cell constants (Å)	$a = 7.5112(10)$ $b = 7.5603(8)$ $c = 8.2185(8)$ $\alpha = 106.904(8)$ $\beta = 94.510(10)$ $\gamma = 113.984(9)$	$a = 14.9340(15)$ $b = 6.4900(9)$ $c = 17.9590(19)$ $\beta = 97.927(12)$
Cell volume (Å^3)	397.51(8)	1724.0(3)
Formula weight (g/entity)	468	501.108
Z/entity	1	4
ρ_{calc} (g cm^{-3})	1.958	1.931
μ (Mo*K*α) (cm^{-1})	12.4	11.77
Dimensions (mm)	$0.15 \times 0.02 \times 0.17$	$0.03 \times 0.17 \times 0.18$
Color	Brown	Green–black
F(000)	210	1016
Wavelength (Mo*K*α) (Å)	0.71073	0.71073
θ_{max} for data collection	32°	30°
Range of *h*, *k*, *l*	(−11,−11,−11) (11,10,12)	(−20,−8,−19)(20,9,25)
Reflections collected	6582	9630
Absorption correction	Sortav	Sortav
Max and min transmission	0.867 and 0.558	0.962 and 0.736
Data/restraints/parameters	2322/0/119	1701/0/129
Goodness-of-fit on F^2	0.942	1.048
Final *R* factor %	$R = 2.8$, w$R = 5.3$	$R = 4.33$, w$R = 11.16$
R factor (all data)	$R = 3.5$, w$R = 5.3$	$R = 7.38$, w$R = 12.52$
Largest peak and hole (e^- Å^{-3})	0.61/−0.74	0.342/−0.439

Table 2
Fractional atomic coordinates and equivalent thermal parameters for $[V(OH)(H_2O)_2(C_4O_4)]_2 \cdot 2H_2O$ **1**

Atom	*x*	*y*	*z*	U_{eq}(Å^2)
V1	0.80824(3)	0.80630(3)	−0.10504(2)	0.01401(8)
O1	0.67664(12)	0.81080(13)	0.09713(11)	0.0211(4)
O2	0.52368(12)	0.79657(12)	0.44277(11)	0.0219(4)
O3	0.92131(13)	1.22828(12)	0.67251(11)	0.0220(4)
O4	1.08963(12)	1.23180(12)	0.32651(11)	0.0204(3)
O5	0.72538(14)	0.50593(12)	−0.15002(11)	0.0241(4)
O6	0.92580(11)	1.11100(11)	−0.04433(10)	0.0171(3)
O7	0.55158(13)	0.75215(15)	−0.24797(12)	0.0311(4)
O8	0.77854(13)	0.38664(13)	0.13530(13)	0.0273(4)
C1	0.74736(16)	0.93118(16)	0.25480(15)	0.0173(4)
C2	0.67364(16)	0.92331(16)	0.41201(15)	0.0172(4)
C3	0.85426(16)	1.11730(16)	0.51602(15)	0.0169(4)
C4	0.92717(16)	1.11788(15)	0.35616(14)	0.0166(4)
H5*a*	0.6531	0.4104	−0.2422	0.0299
H5*b*	0.7126	0.4523	−0.0740	0.0299
H6	0.9192	1.1460	−0.1417	0.0244
H7*a*	0.4502	0.7079	−0.2157	0.0371
H7*b*	0.5382	0.7591	−0.3490	0.0371
H8*a*	0.8697	0.4943	0.1958	0.0330
H8*b*	0.8217	0.2986	0.0976	0.0330

Table 3
Fractional atomic coordinates and equivalent thermal parameters for $(NH_4)[(VO)_2(OH)(C_4O_4)_2(H_2O)_3] \cdot 3H_2O$ **2**

Atom	*x*	*y*	*z*	U_{eq} (Å^2)	Occupation factor
V	0.00981(3)	0.13735(7)	0.15654(2)	0.02991(17)	1
O1	0.14281(11)	0.1829(3)	0.18312(10)	0.0337(4)	1
O2	0.35588(12)	0.1372(3)	0.22302(11)	0.0351(4)	1
O3	0.33466(12)	0.1037(3)	0.40297(11)	0.0397(5)	1
O4	0.12441(11)	0.1705(3)	0.36450(10)	0.0326(4)	1
O5	0.01652(14)	−0.0471(4)	0.09958(11)	0.0471(5)	1
O6	0	−0.0063(4)	1/4	0.0314(6)	1
O7	0	0.3916(4)	1/4	0.0285(5)	1
O8	0.01184(12)	0.3858(3)	0.08774(11)	0.0394(5)	1
O9	0.35690(15)	0.1153(3)	0.06737(12)	0.0474(5)	1
O10	0.17409(16)	0.0081(4)	0.01290(13)	0.0515(6)	0.5
N	0.17409(16)	0.0081(4)	0.01290(13)	0.0515(6)	0.5
C1	0.19513(15)	0.1640(4)	0.24514(14)	0.0267(5)	1
C2	0.29330(15)	0.1429(4)	0.26204(15)	0.0271(5)	1
C3	0.28465(15)	0.1297(4)	0.34321(14)	0.0282(5)	1
C4	0.18693(15)	0.1569(4)	0.32350(14)	0.0269(5)	1
H6	0	−0.1295	1/4	0.038	1
H7	0.0450	0.4747	0.2455	0.034	1
H8*a*	−0.0419	0.4596	0.0741	0.047	1
H8*b*	0.0638	0.4722	0.0914	0.047	1
H9*a*	0.3561	0.1430	0.1178	0.057	1
H9*b*	0.3109	0.0307	0.0460	0.057	1

the vanadium entity, was occupied equally by an ammonium ion and by a water molecule. Such an assignment was consistent with the *U* values on the two sites. Hydrogen atoms were not localized on this mixed site.

The final reliability factors converged to $R_{obs} = 2.8$, 4.33% and w$R_{obs} = 5.3$, 11.16% for compounds **1** and **2**, respectively. The final atomic and equivalent thermal parameters, with estimated standard deviations, are listed in Tables 2 and 3. Selected bond lengths and

Table 4
Selected interatomic distances (Å) and angles(deg) for $[V(OH)(H_2O)_2(C_4O_4)]_2 \cdot 2H_2O$ **1**

Around V						
V–O6	1.986(2)		V–O5	2.002(2)		
V–O7	1.997(3)		V–O6^{i}	2.010(2)		
V–O1	1.998(2)		V–O4^{i}	2.020(2)		
O1–V–O4^{i}	172.80(10)	O1–V–O5	87.52(10)		O1–V–O6	93.56(10)
O1–V–O6^{i}	92.42(10)	O1–V–O7	87.53(11)		O4^{i}–V–O5	87.38(10)
O4^{i}–V–O6	92.17(10)	O4^{i}–V–O6^{i}	92.79(10)		O4^{i}–V–O7	87.74(11)
O5–V–O6	172.35(11)	O5–V–O6^{i}	91.69(10)		O5–V–O7	93.62(12)
O6–V–O6^{i}	80.70(10)	O6–V–O7	93.99(11)		O6^{i}–V–O7	174.68(10)
V–O6–V^{i}	99.30(10)	V–O6^{i}–V^{i}	99.30(10)			
Squarate						
O1–C1	1.266(4)		C1–C2	1.453(5)		
O2–C2	1.249(4)		C1–C4	1.449(4)		
O3–C3	1.241(4)		C2–C3	1.481(4)		
O4–C4	1.267(4)		C3–C4	1.463(5)		
O1–C1–C2	131.8(3)	O2–C2–C3	136.4(3)		C2–C3–C4	88.9(2)
O1–C1–C4	137.5(3)	C1–C2–C3	89.8(2)		O4–C4–C1	136.2(3)
C2–C1–C4	90.6(2)	O3–C3–C2	136.0(3)		O4–C4–C3	133.0(3)
O2–C2–C1	133.8(3)	O3–C3–C4	135.0(3)		C1–C4–C3	90.6(2)

Hydrogen bonding or Van der Waal interactions

	D–H	H···*A*	*A*···*D*	*D*–H···*A*
O5–H5*a*···O2^{ii}	0.83	1.84	2.6708(13)	175.5
O5–H5*b*···O8	0.83	2.00	2.8013(14)	161.0
O6–H6···O3^{iii}	0.92	1.81	2.7231(12)	176.5
O7–H7*a*···O8	0.80	1.83	2.6301(15)	178.2
O7–H7*b*···O2^{iii}	0.85	1.82	2.6622(13)	175.5
O8–H8*a*···O3^{iv}	0.80	1.94	2.7355(14)	173.1
O8–H8*b*···O6^{v}	0.85	2.02	2.8438(14)	165.6

Symmetry code:
i: $-x+2, -y+2, -z$; ii: $-x+1, -y+1, -z$; iii: $x, y, z-1$; iv: $-x+2, -y+2, -z+1$; v: $x, -y+1, z$; vi: $x, y, z+1$.

angles are given in Tables 4 and 5 for **1** and **2**, respectively.

3. Results and discussion

3.1. Structure of $[V(OH)(H_2O)_2(C_4O_4)]_2 \cdot 2H_2O$ 1

The asymmetric unit of the compound **1** is shown in Fig. 1a. The vanadium atom is six coordinated with an octahedral geometry. The V–O bond lengths range from 1.986(2) to 2.020(2) and are compatible with a V(III) compound. Although V_2O_5 was used for the preparation, the formation of the V(III) ion can be attributed to the reductive properties of the squarate ion. Firstly, the presence of V(III) is corroborated by the crystalline structure study where two protons are located near O5 and O7 water oxygen atoms, and only one proton near O6 hydroxyl one. Secondly, bond valence sum calculated from the bond distances by means of the Altermatt and Brown method gives 2.98 [17]. Finally, a study of the magnetic properties of this compound confirms this result (see later).

This structure is made of discrete, neutral, bimetallic entities $[V(OH)(H_2O)_2(C_4O_4)]_2 \cdot 2H_2O$ in which the vanadium octahedra share the edge O6–O6^{i} (i: $-x+2, -y+2, -z$). Within this entity, the V–V^{i} is 3.046(1) Å. The squarate ligand is coordinated in a μ_2 mode to the two vanadium atoms of the dimer via the oxygen atoms, O1 and O4 (see Fig. 1). The squarate retains two shorter C–O distances (C2–O2 and C3–O3, see Table 4), corresponding to oxygen atoms not coordinated to vanadium atoms.

As shown in Fig. 2, the bimetallic vanadium entities are nearly parallel to the $(-1-10)$ plane. The distance C3–C3^{iv} = 3.314(3) Å involves some Van der Waals interactions, due to the aromatic feature of the squarate species [18,19].

The crystal structure arises from hydrogen bonding between squarate oxygen atoms, water molecules and hydroxyl groups. All the water molecules and the hydroxyl groups are involved in strong hydrogen bonding. The distances between the donor atom and the acceptor atom range from 2.630(2) to 2.844(1) Å and the angles O–H···O range from 161.0° to 176.4° (Table 4).

Table 5
Selected interatomic distances (Å) and angles (deg) for $(NH_4)[(VO)_2(OH)(C_4O_4)_2(H_2O)_3]\cdot 3H_2O$ **2**

Around V					
V–O5	1.587(2)			V–O1	1.9997(17)
V–O6	1.9432(14)			V–O8	2.034(2)
V–O4^{i}	1.9994(17)			V–O7	2.3726(19)
V–V^{i}	3.4097(4)				
O5–V–O6	102.35(11)	O4^{i}–V–O1	165.02(9)	O5–V–O7	175.07(10)
O5–V–O4^{i}	96.32(9)	O5–V–O8	101.47(11)	O6–V–O7	72.74(8)
O6–V–O4^{i}	91.25(6)	O6–V–O8	156.09(10)	O4^{i}–V–O7	84.31(6)
O5–V–O1	96.69(9)	O4^{i}–V–O8	84.17(8)	O1–V–O7	83.37(6)
O6–V–O1	93.18(6)	O1–V–O8	86.00(8)	O8–V–O7	83.45(8)
V–O6–V^{i}	122.65(14)	V–O7–V^{i}	91.87(9)		
Squarate					
O1–C1	1.275(3)			C1–C4	1.430(4)
O2–C2	1.244(3)			C1–C2	1.462(3)
O3–C3	1.232(3)			C2–C3	1.483(4)
O4–C4	1.270(3)			C3–C4	1.464(3)
O1–C1–C4	137.5(2)	O2–C2–C3	136.6(2)	C4–C3–C2	88.53(18)
O1–C1–C2	131.8(2)	C1–C2–C3	89.36(18)	O4–C4–C1	137.6(2)
C4–C1–C2	90.69(18)	O3–C3–C4	133.8(2)	O4–C4–C3	131.0(2)
O2–C2–C1	134.1(2)	O3–C3–C2	137.7(2)	C1–C4–C3	91.38(19)
Hydrogen bonding or Van der Waal interaction					
	D–H	H···*A*	*A*···*D*	*D*–H···*A*	
O6–H6···O2^{ii}	0.80	2.62	3.151(3)	125.3	
O6–H6···O2^{iii}	0.80	2.62	3.151(3)	125.3	
O7–H7···O2^{iv}	0.87	1.84	2.668(2)	157.0	
O8–H8*a*···O9^{v}	0.94	1.81	2.734(3)	168.6	
O8–H8*b*···O3^{iv}	0.95	1.73	2.679(3)	173.4	
O9–H9*a*···O2	0.92	1.89	2.801(3)	167.6	
O9–H9*b*···N	0.92	2.05	2.856(3)	145.0	
N–O9^{vi}	2.843(3)			N–O4^{vii}	2.907(3)
N–O5	3.016(3)			N–O3^{iii}	3.040(3)

Symmetry code:
i: $-x, y, -z+1/2$; ii: $x-1/2, y-1/2, z$; iii: $-x+1/2, y-1/2, -z+1/2$; iv: $-x+1/2, y+1/2, -z+1/2$; v: $x-1/2, y+1/2, z$; vi : $-x+1/2, -y+1/2, -z$; vii: $x, -y, z-1/2$; viii: $x+1/2, y+1/2, z$.

According to the coordination mode of the squarate anion different dimensionalities can be obtained. A molecular structure of a binuclear tin(IV)-squarate, $[(n\text{–}C_4H_9)_4N]_2[Sn_2Cl_4(OCH_3)_2(C_4O_4)_2]$ [20] has been obtained when the squarate is coordinated in a μ_2 mode, like in our compounds. When it is coordinated in a μ_3 mode (to two dimers) it gives a layer structure as for the compound $[\{V(OH)(C_4O_4)(H_2O)_2\}]$ [8]. Finally, a three-dimensional framework, with large square channels, can be obtained as for example in $[\{V(OH)(C_4O_4)\}_2]\cdot 4H_2O$, when the squarate is coordinated in a μ_4 mode (to four dimers) [8]. Considering these results a higher coordination of the squarate ion seems to favor the formation of open framework structures.

3.2. Structure of $(NH_4)[(VO)_2(OH)(C_4O_4)_2(H_2O)_3]\cdot 3H_2O$ **2**

The structure of **2** consists of discrete bimetallic entities, $[(VO)_2(OH)(H_2O)_3(C_4O_4)_2]$, and presents the same topology as for **1** (Fig. 1b). However, the dimeric vanadium entity bears one negative charge which is balanced by the presence of one ammonium cation.

The vanadium atom is bound to six oxygen atoms at distances ranging from 1.587(2) to 2.372(2) Å. The shortest distance is characteristic of a vanadyl bond, indicating that vanadium atoms are present at an oxidation state +IV. Such a valence is an agreement with the calculation of bond valence sum which gives 4.18 [17]. The coordination polyhedron observed for V(+IV) is a distorted octahedron or a square bi-pyramid. The six-coordinate geometry [4+1+1] consists of four intermediate equatorial bonds (1.943(1) Å–2.034(2) Å), one short axial bond (1.587(2) Å–O5) and a long axial bond (2.372(2) Å–O7, water molecule) (Table 5). The equatorial bonds are decomposed into one hydroxyl group (O6), two squarate oxygen atoms (O1 and O4^{i}) and one water molecule (O8). The O5–V–O7 angle is 175.1(1)° and the equatorial angles range from 84.18(8)° to 93.18(6)° (Table 5). Within its octahedron, the vanadium atom is displaced by 0.361(2) Å above the equatorial plane, O1O7O4^{i}O6, toward O5. Two

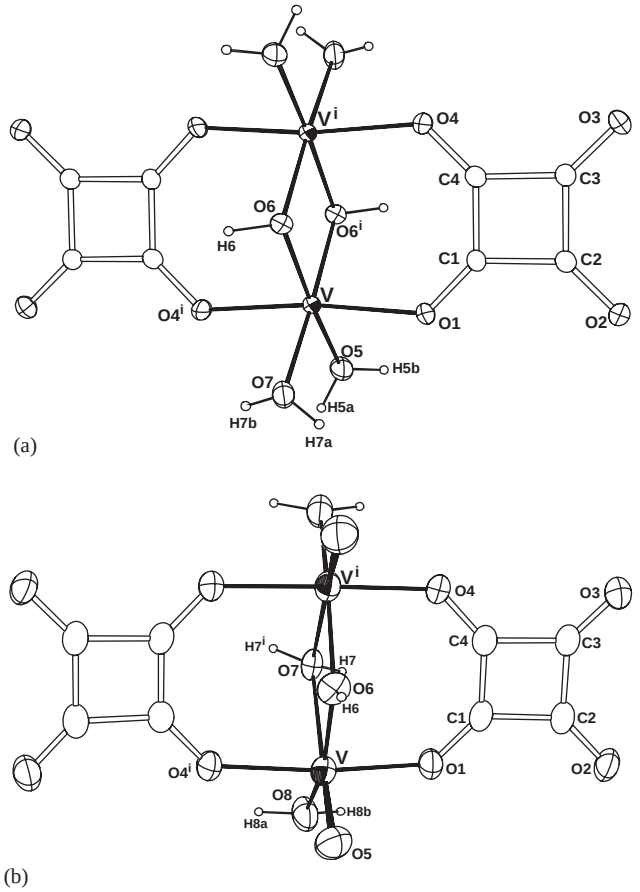

Fig. 1. View of the bimetallic vanadium entity with labeling scheme, (a) for **1** and (b) for **2**. The symmetry codes are given in Tables 4 and 5 for **1** and **2**, respectively. The thermal displacement parameters are 50%.

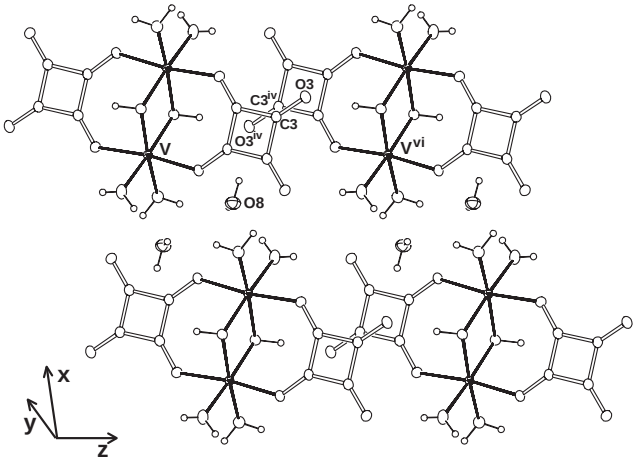

Fig. 2. Projection on the (−1–10) plane of the stacking of the bimetallic vanadium entities for **1**. The symmetry codes are given in Table 4.

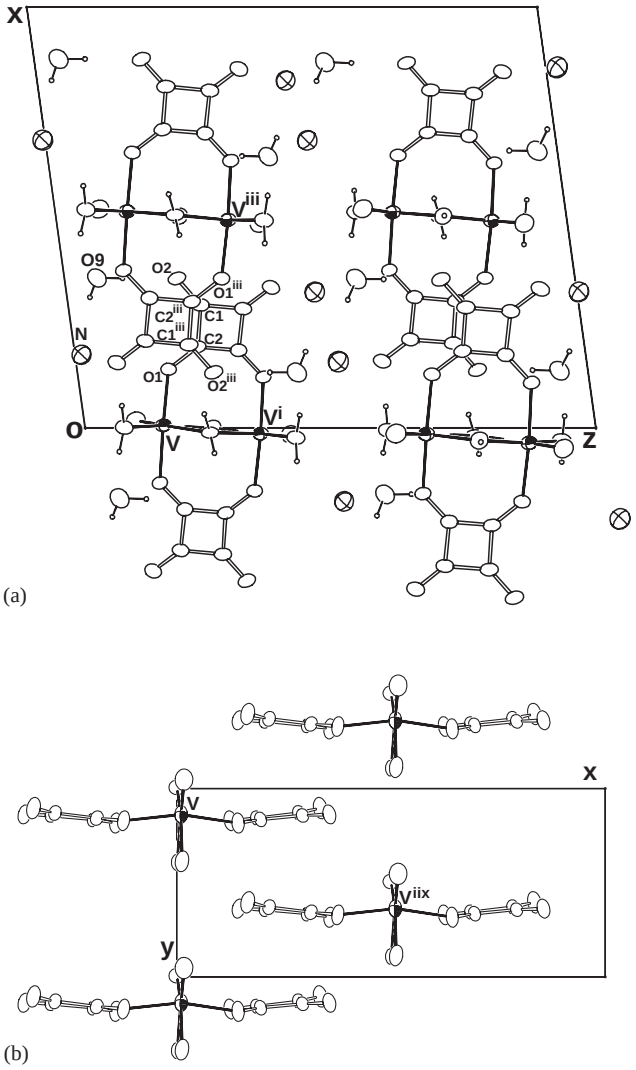

Fig. 3. (a) View, along *b*, of the two layers formed by the stacking of the vanadium entities which sandwiched the free water molecule and the ammonium ion (in this mixed site, O10 and N, only N will be represented) for **2**. (b) Projection, along *c*, of the stacking of the squarate ions for **2**. The symmetry codes are given in Table 5.

octahedra share the edge O6–O7 which are localized on the binary axis. Within such a dimer, the V–V^{i} distance is equal to 3.4097(4) Å and the angles V–O6–V^{i} and V–O7–V^{i} are 122.6(1)° and 91.87(9)°, respectively. An angle of approximately 82.1° is observed between the vanadyl vectors.

The squarate ligand acts as terminal part of the vanadium entity. As for compound **1**, squarate is coordinated in a μ_2 mode to the two vanadium atoms via the oxygen atoms, O1 and O4. Such a coordination mode, results in a slight trapezoid deformation of the carbon ring with C1–C4 bond 0.052 Å shorter than C2–C3, the other C–C bonds keep the usual value (1.46 Å) [21,22]. Likely for the C–O distances, the C–O linked to the vanadium are longer ($\Delta = 0.026–0.042$ Å) than the opposite ones (Table 5). The carbon ring is planar within 0.010(1) Å, if the oxygen atoms are included, atoms to mean plane deviations reach

0.038(2) Å. The squarate ions stack up along *y*-axis (Fig. 3a and b). A dihedral angle of 14.06(2)° was observed between the planes of neighboring ligands. As shown from the Fig. 3a, there is an overlap of the bond C1–C2 and the distances C1–C2^{iii} or C2–C1^{iii} (3.389(4) Å or 3.117(4) Å, respectively) are likely to result from some Van der Waals interactions, due to the aromatic character of the squarate species [18,19]. These interactions lead to a layer parallel to the (001) plane. The cohesion of such layer is strengthened by strong hydrogen bonding via the water molecules, O7 and partially O8 (Table 5). The hydroxyl group O6, is not involved in strong hydrogen bonding. The free water molecule O9, and the ammonium ion are sandwiched between two layers. Although hydrogen was not localized on the ammonium ion, this one is probably related by hydrogen bonding to the neighboring layers. Some possible interactions between the ammonium ion or the water molecule O10 and the oxygen atoms of the vanadium entity are listed in Table 5.

It is worth to mention that this binuclear vanadium(IV) species **2** is in fact very similar to those described in Refs. [9,11], namely $(NH_4)[(VO)_2(OH)(C_4O_4)_2(H_2O)_3]\cdot H_2O$ (blue crystals) noted here **2′** and $Na[(VO)_2(OH)(C_4O_4)_2(H_2O)_3]\cdot 6H_2O$. The main difference between **2** and **2′** concerns the number of water molecules of crystallization: three for **2** and one for **2′**. Despite structural similarity, the following comments must be made. Both structures crystallize in the monoclinic system: $C2/c$ for **2**, but a discrepancy is evident in Ref. [9]. The structure of **2′** was described in the space group $P2_1/n$ in the abstract and $P2_1/m$ in the Table 1. Strange enough is that neither $P2_1/n$ nor $P2_1/m$ are compatible with the positional parameters. In fact, this structure could be probably described in the non-centrosymmetric space group $P2_1$ as indicated by the *y* coordinate of V1 atom fixed at 1/2.

Another point to note concerns the volume of the two varieties. Form **2** is more hydrated than **2′**, however the volume per entity is lower in **2** compare to **2′** (431 and 483 Å^3, respectively). As a consequence, the density of **2′**, 1.638 g/cm^3, is lower than the one of **2**, 1.93 g/cm^3 (this latter one being comparable to the sodium derivative, 1.91 g/cm^3 [11]) which indicates that the phase isolated by Khan et al. appears as a more open-structure [9].

3.3. Thermal behavior

For **1**, the total weight loss agrees well with the formula assuming that the final product is V_2O_5 (obs. 61.5%, calc. 61.14%). Two weight losses are observed. The first one corresponding to four water molecules per bimetallic vanadium entity (obs. 15.1%, calc. 15.38%) occurs very smoothly at 100°C and it ends up by an inflexion point around 180°C. Such dehydration process can be attributed to the free water molecules (two O8) and to two molecules of the entity. The second loss consists in two stages which are not well resolved. It starts at 180°C and terminates around 260°C. It corresponds to the departure of the remaining species and to the decomposition of the squarate ligand (obs. 46.4%, calc. 45.76%).

The thermal behavior for **2** is in good agreement with the formula, leading to V_2O_5 (obs. 63.3%, calc. 63.70%). There are roughly three weight losses. The second and the third ones consisting of two stages which are overlapping. The first loss, between 50°C and 110°C, can be attributed to two water molecules (obs. 6.7%, calc. 7.18%) per vanadium entity, probably O9 which is the less bound to the lattice. The second loss, between 120°C and 220°C, can also been interpreted as dehydration step (one O7 + two O8 + one O10; obs. 14.4%, calc. 14.37%). The third loss, between 220°C and 370°C, is attributed to the departure of the remaining hydrogenated species ($NH_4^+ + OH^-$) and to the decomposition of the squarate ligand leading to V_2O_5 (obs. 42.3%, calc. 42.15%).

It is important to notice that the thermal analyses of **1** and **2** are in agreement with their detailed structures: (i) For **1**, all the hydroxyl groups or the water molecules are involved in strong hydrogen bonding while for **2**, these interactions are weaker. This is the reason why for **1**, the dehydration process starts around 100°C while for **2**, it starts around 50°C. (ii) for **1**, the decomposition of squarate ligand is ranging from 180°C to 270°C while for **2**, it is shifted towards higher temperature, from 220°C to 370°C. This difference might be related to the vanadium valence, +III and +IV for **1** and **2**, respectively. It is known that the vanadium +III is easily oxidized. The oxidation of vanadium +III will therefore induces the decomposition of the squarate ligand at relatively lower temperature compared to vanadium +IV. For $M(C_4O_4)\cdot 2H_2O$ with M = Ni, Fe, Mn, Zn, Cu and Co, it has been observed that the decomposition of the squarate ligand can range from 250°C to 350°C depending on their relevant cation M [23].

3.4. Infrared

The infrared spectra of **1** and **2** are presented in Fig. 4. Both spectra exhibit the characteristic bands of the squarate ligand which are not strictly at the same wave number for **1** and **2**: around 1620 cm^{-1} ν(C–O), 1520 cm^{-1} ν(C–C) and 1110–1090 cm^{-1} ν(C–C) of the carbon ring [24,25]. Moreover a sharp band around 1820 cm^{-1}, attributed to ν(C=O), as well as a strong massif of water around 3395 cm^{-1} and 3150 cm^{-1} are present in these spectra. However there are some marked differences between these spectra. (i) The band observed for **1** and attributed to ν(V–O) at 874 cm^{-1} is

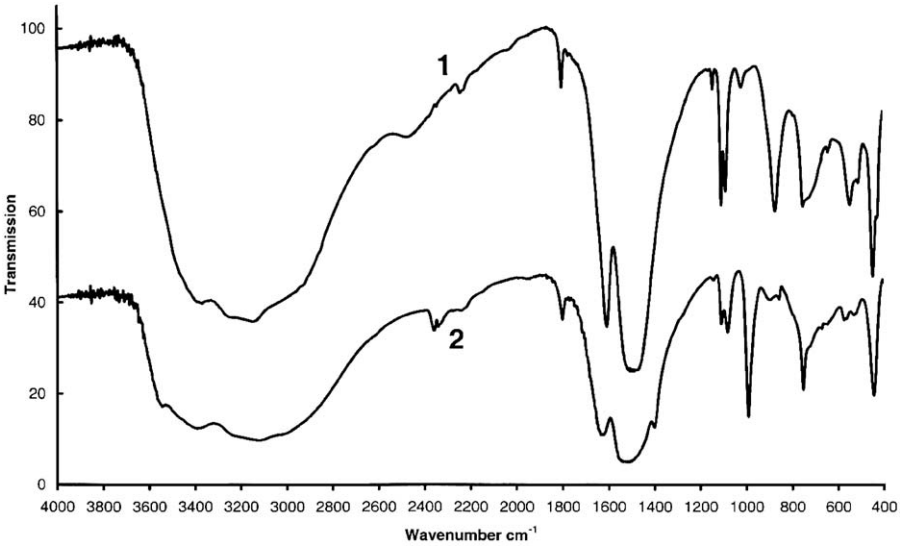

Fig. 4. Infrared spectra of compounds **1** and **2**.

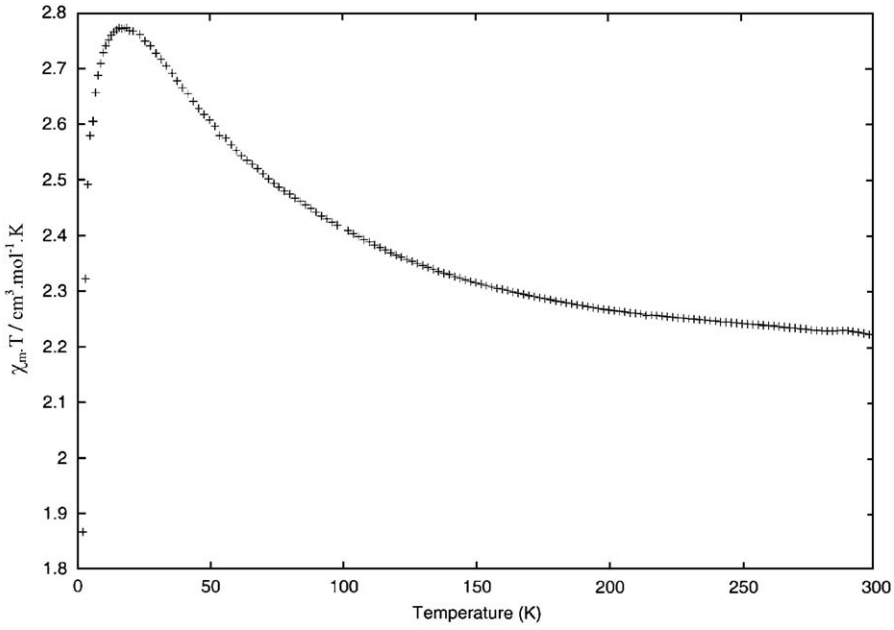

Fig. 5. Plot of the molar susceptibility time temperature versus temperature for **1**.

shifted towards the high wave numbers at 990 cm^{-1} for **2** and is characteristic of the V = O stretching band [26]. (ii) For the compound **2**, a band at 1415 cm^{-1} which is absent for **1**, is relevant to the presence of $(NH_4)^+$ ion, δ(N–H). However, it is difficult to see the stretching band of such an ion around 3145 cm^{-1}, in presence of a lot of water. (iii) For the compound **2**, the presence of a sharp band at 3565 cm^{-1} ascribed to ν(O–H) of the hydroxyl groups. We have observed that the hydroxyl groups are involved in a strong hydrogen bonding for **1** while for **2** they are not. The effect of such a strong hydrogen interaction for **1** shifts the wave number towards the low value and consequently they can be quite indistinguishable from the water massif [27].

3.5. Magnetic properties

The magnetic susceptibility of **1** as a function of temperature shows a Curie–Weiss behavior with the positive Weiss temperature $\theta \sim 10$ K. This indicates ferromagnetic interactions between the spin moments of vanadium(III) ($S = 1$). This is clearly visible on the $\chi_m \cdot T$ versus T plot in Fig. 5, with at $T_{max.} \sim 18.5$ K the appearance of a $S = 2$ ground state characteristic of

ferromagnetic coupling of $3d^2$, $S=1$ states. The decrease of $\chi_m \cdot T$ at lower temperatures is mainly due to inter-binuclear species interactions. The presence of ferromagnetic exchange interactions in **1** can be accounted for by the local coordination around the vanadium(III) forming the dimer. The angles V–O6(O6^i)–V^i are both equal to 99.3(1)°. If this compound was based on copper(II), such V–O(hydroxo)–V angles would lead to anti-ferromagnetic interactions. However if one looks carefully at the orbital imparted in the super-exchange interactions, one can notice that the V–O overlap is of π type for vanadium compare to σ for copper(II). That leads for compound **1** to a super-exchange contribution much smaller than in the copper case and therefore direct exchange (always ferromagnetic) must prevail even for this value 99° of V–O–V angle. Ab initio calculations will be performed to confirm such assumption.

In the case of compound **2**, anti-ferromagnetic exchange interaction is expected owing to the strong similarity between **2** and $(NH_4)[V_2O_2(OH)(C_4O_4)_2(H_2O)_3]\cdot H_2O$ [9]. In this latter case, density functional theory (DFT) combined with broken-symmetry approach [28] highlighted the correlation between the V–O(hydroxo)–V angle, the V–O(hydroxo) distance and the exchange coupling constant J. It was shown that the bridging hydroxo ligand is the most sensitive part for the anti-ferromagnetic coupling between the two vanadium(IV) sites. In addition one can notice in **2** that V–O7–V^i and V–O6–V^i angles are respectively close to 90° and 120°. Therefore no super-exchange path is expected via O7 while a strong super-exchange contribution might be present via O6 resulting in anti-ferromagnetic coupling between the two vanadium(IV) sites. Magnetic susceptibility measurements will be performed as soon as pure sample can be isolated.

4. Conclusion

As a part of our investigations, two binuclear vanadium (III) and (IV) squarate forms, which were different from the comparable species described in literature data, have obtained From a chemical and crystallographical point of view, it will be suitable to modify the dimensionality of such dimers by adding for example another inorganic or organic cation. The magnetic properties of form **1** indicate the presence of ferromagnetic interaction not so common for vanadium(III) binuclear species. Ab initio calculation will be performed to analyze this puzzling effect.

Acknowledgments

Thanks are due to J. Bonvoisin, J. Jaud, Y. Khin, M.B. Lepetit and P. Salles for fruitful discussions.

References

[1] M.S. Whittingham, MRS Bull. 29 (1989) 31–38.
[2] J. Galy, J. Solid State Chem. 100 (1992) 209–245.
[3] P.J. Hagrman, D. Hagrman, J. Zubieta, Angew. Chem. Int. Ed. 38 (1999) 2638–2684.
[4] S.O.H. Gutschke, M. Molinier, A.K. Powell, P.T. Wood, Angew. Chem. Int. Ed. 36 (1997) 991–992.
[5] S. Neeraj, M.L. Noy, C.N.R. Rao, A.K. Cheetham, Solid State Sci. 4 (2002) 1231–1236.
[6] A. Weiss, E. Riegler, C. Robl, Z. Naturforsch. 41b (1986) 1329–1332.
[7] K. Barthelet, J. Marrot, D. Riou, G. Férey, Angew. Chem. Int. Ed. 41 (2002) 281–284.
[8] K-J. Lin, K-H. Lii, Angew. Chem. Int. Ed. 36 (1997) 2076–2077.
[9] M.I. Khan, Y-D. Chang, Q. Chen, J. Salta, Y-S. Lee, C.J. O'Connor, J. Zubieta, Inorg. Chem. 33 (1994) 6340–6350.
[10] D.S. Yufit, D.J. Price, J.A.K. Howard, S.O.H. Gutschke, A.K. Powell, P.T. Wood, Chem. Comm. 16 (1999) 1561–1562.
[11] A. Müller, R. Rohlfing, E. Krickemeyer, H. Bögge, Angew. Chem. Int. Ed. 32 (1993) 909–912.
[12] K. Yvon, W. Jeitschko, E. Parthe, J. Appl. Crystallogr. 10 (1977) 73–74.
[13] A. Altomare, G. Cascarano, C. Giacovazzo, A. Guagliardi, M.C. Burla, G. Polidori, M. Camalli, J. Appl. Cryst. 27 (1994) 1045–1050.
[14] R.H. Blessing, Acta Cryst. A 51 (1995) 33–38.
[15] S. Mackay, C.J. Gilmore, C. Edwards, N. Stewart, K. Shankland, Maxus Computer Program for the Solution and Refinement of Crystal Structures, Nonius, The Netherlands, MacScience, Japan and the University of Glasgow, 1999.
[16] G.M. Sheldrick, SHELXL97 Program for the Refinement of Crystal Structures, University of Göttingen, Germany, 1997.
[17] D. Altermatt, I.D. Brown, Acta Cryst. B 41 (1985) 240–244.
[18] W.M. Macintyre, M.S. Verkema, J. Chem. Phys. 42 (1964) 3563.
[19] J.F. Petit, A. Gleizes, J.C. Trombe, Inorg. Chim. Acta 167 (1990) 51–68.
[20] Q. Chen, S. Liu, J. Zubieta, Inorg. Chim. Acta 175 (1990) 269–272.
[21] R. West, H.Y. Niu, J. Am. Chem. Soc. 85 (1963) 2589–2590.
[22] C.-R. Lee, C.-C. Wang, Y. Wang, Acta Cryst. B 52 (1996) 966–975.
[23] R.A. Bailey, W.N. Mills, W.J. Tangredi, J. Inorg. Nucl. Chem. 33 (1971) 2387–2393.
[24] M. Ito, R. West, J. Am. Chem. Soc. 85 (1963) 2580–2584.
[25] F.G. Baglin, C.B. Rose, Spectrochim. Acta A 26 (1970) 2293–2304.
[26] K. Nakamoto, Infrared Spectra of Inorganic and Coordination Compounds, Wiley-Interscience, New York, 1970.
[27] W.C. Hamilton, J.A. Ibers, In Hydrogen Bonding in Solids, W.A. Benjamin Inc., New York, 1968.
[28] L. Zhang, Z. Chen, Chem. Phys. Lett. 345 (2001) 353–360.